Research Article | Vol. 27, No. 11 | 27 May 2019 | OPTICS EXPRESS 15391
Optics EXPRESS

Electrically switchable photonic crystals based on liquid-crystal-infiltrated TiO_2-inverse opals

YING ZHANG,[1] KE LI,[1] FENGYU SU,[1,2] ZHONGYU CAI,[3,7] JIANXUN LIU,[1,4] XIAOWEN WU,[5] HUILIN HE,[1] ZHEN YIN,[1] LIHONG WANG,[1] BING WANG,[4] YANQING TIAN,[5] DAN LUO,[1] XIAO WEI SUN,[1,6] AND YAN JUN LIU[1,6,*]

[1]*Department of Electronic and Electrical Engineering, Southern University of Science and Technology, Shenzhen 518055, China*
[2]*SUSTech Academy for Advanced Interdisciplinary Studies, Southern University of Science and Technology, Shenzhen 518055, China*
[3]*Department of Chemistry, University of Pittsburgh, Pittsburgh, PA 15260, USA*
[4]*Wuhan National Laboratory for Optoelectronics and School of Physics, Huazhong University of Science and Technology, Wuhan 430074, China*
[5]*Department of Materials Science and Engineering, Southern University of Science and Technology, Shenzhen 518055, China*
[6]*Shenzhen Planck Innovation Technologies Pte Ltd, Ganli 6th Road, Longgang, Shenzhen 518112, China*
[7]*zhc35@pitt.edu*
**yjliu@sustech.edu.cn*

Abstract: Electrically switchable photonic crystals are demonstrated based on TiO_2 inverse opals infiltrated with liquid crystals. Macroporous anatase TiO_2 inverse opals are fabricated from polystyrene opal templates through a sandwich vacuum backfilled method and followed by calcination. Upon liquid crystal infiltration, the optical properties of the hybrid organic/inorganic structure are characterized by reflectance measurements of the Bragg peak, the position of which can be switched using an external electric field. The physical mechanism underlying this switchable behavior is the reorientation of the liquid crystal molecules inside the spherical voids by the applied electric field, resulting in a significant change of the refractive index contrast between the liquid crystal and the TiO_2 inverse opal. With advantageous features of cost-effective fabrication, easy integration, and electric control, such TiO_2 inverse opals infiltrated with liquid crystals could play an important role in future development of active photonic devices.

1. Introduction

Photonic crystals (PhCs) that enable the molding of the flow of photons [1], hold the great promise for an emerging generation of micro-/nano-scale optoelectronic components. Opals and inverse opals (IOs) are a kind of three-dimensionally (3D) ordered PhCs [2,3], which are prepared by the self-assembly of monodispersed colloidal particles and their derivatives. Upon the light incidence, interferences between strongly scattered waves lead to a modification of the photon density of states in particular wavelength regions [4]. In recent years, they have attracted growing interest for many potential applications including optoelectronic devices (optical switches or lasers) [5–7], sensing [8,9], protein patterning [10], and so on. The performance of these devices is mainly related to the lattice periodicity, the quality and the size of the ordered structure and the refractive index contrast.

Recently, titanium dioxide inverse opals (TiO_2–IO) PhCs have gained particular attention because of its excellent optical and electronic properties [11–15]. Based on the slow photon effect, TiO_2–IO PhCs have demonstrated greatly enhanced photocatalytic and photovoltaic

#359170 https://doi.org/10.1364/OE.27.015391
Journal © 2019 Received 31 Jan 2019; revised 4 May 2019; accepted 5 May 2019; published 15 May 2019

Optics EXPRESS

activity [16–19]. Especially, anatase TiO_2 has shown excellent potential on the treatment of industrial wastewater containing harmful aromatic compounds and organic dyes [20–22].

However, many potential applications of PhCs require active control over the photonic bandgap (PBG) structure through external stimuli. The PBG tuning is mainly related with the lattice constants and the refractive index. In recent years, it has been reported that various approaches have been exploited to tune the PBG, including the volume phase transition of hydrogels by controlling the temperature or the pH [23,24], electrically [25–27] and optically [28–32] controlled birefringence of liquid crystal, etc. However, the low index contrast in the LC-infiltrated SiO_2-IO material system greatly limits the optical performance. Instead, high index contrast in the LC-infiltrated PhCs is highly desirable to enhance its optical performance.

In this study, we report an electrically switchable PhC based on LC-infiltrated TiO_2-IOs. The TiO_2-IOs was fabricated via a sandwich-vacuum technique by utilizing self-assembled polystyrene (PS) colloidal spheres as the template [33]. Upon LC infiltration, the large voids inside the TiO_2-IOs provide the low anchoring energy for the LC molecules due to the relatively low surface-to-volume ratio, hence facilitating the easy control of the LC molecules' alignment. Driven by an external electric field, the LC molecules can be realigned, showing a large change of the refractive index and hence leading to switchable Bragg reflection. With facile and cost-effective fabrication, such an electrically switchable PhC holds great potential for many applications including structural colors, optical filters, etc.

2. Experimental

2.1 Chemicals

All reagents and solvents were purchased from commercial suppliers and used without further purification unless specified. Styrene (St, analytically pure) and potassium persulfate (KPS, analytical pure) were purchased from Energy Chemical Reagent Co. Deionized water (> 18.2 MΩ cm) was used in all polymerization processes of this study. Titanium (IV) butoxide (97%, Sigma-Aldrich) was purchased from Aladdin.

2.2 Synthesis of PS microspheres

An emulsifier-free emulsion polymerization approach was used to synthesize monodisperse PS colloidal microspheres [34]. The polymerization was carried out in a four-necked jacked glass reactor equipped with nitrogen bubbler. Deionized (DI) water (100 mL) was firstly introduced into the glass reactor purged with nitrogen for 10 min. Then, styrene was added into the reactor, and mixture was stirred vigorously at 330 rpm for another 10 min below 70°C. A small amount of KPS aqueous solution was added, and the polymerization reaction was carried out at 70°C for 20 h with nitrogen protection. After that, the mixture was cooled down to room temperature and filtered to remove coagulum. The filtrate was kept for the following experiment.

2.3 Fabrication of PS opal films

All substrates (FTO) were subsequently cleaned with acetone, ethanol and DI water in an ultrasonic bath for 15 min, and then treated with O_2 plasma for 15 sec. Then the FTO glass substrates were washed with copious DI water and dried under nitrogen gas prior to use [35]. PS colloidal spheres with the size of 200 nm and 250 nm in diameter were synthesized for the present study. PS colloidal crystals (opal) films were self-assembled on FTO substrates via a vertical deposition method [36].

2.4 Fabrication of TiO_2 inverse opals

10 mL of titanium (IV) butoxide, 10 mL anhydrous ethanol and 1 mL nitric acid were vigorously stirred for 30 minutes to obtain homogenous titanium (IV) butoxide sol. Before

infiltration with the TiO_2 precursor solution, the PS opal films were annealed at 80 °C for 20 min. A sandwich-vacuum technique was employed for the infiltration (Fig. 1) [33]. Typically, the PS opal films template was covered with a smooth glass slide and pressed together with two clips. The close contact between the opal template and the glass slide may avoid the formation of a TiO_2 overlayer. Then half of the template was immersed in the modified TiO_2 precursor solution, and the other half was exposed to air. The container holding the TiO_2 precursor solution was sealed with a stopper and connected to a vacuum pump. After infiltration, the opal/TiO_2 composite was allowed to dry for 24 h in air. Then the samples were calcined at 450 °C with a ramp rate of 1°C/min and kept at 450 °C for 4 h. After selectively removing the PS opals via calcination, anatase TiO_2-IO with a well-ordered open macroporous structure were obtained [33].

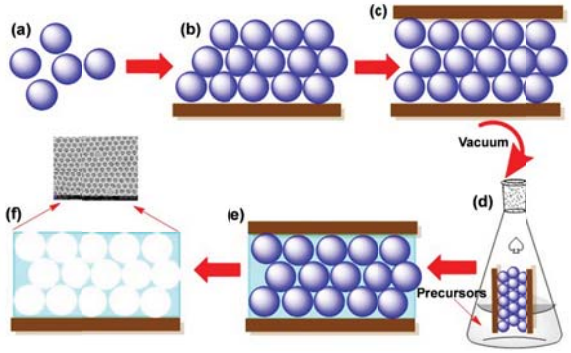

Fig. 1. Schematic illustration of the fabrication of TiO_2 inverse opals.

2.5 LC infiltration

Once the TiO_2-IO films were ready, we assembled them with the bare ITO glass substrates to form a LC cell. The thickness was controlled to be ~20 μm using the PS microspheres. The LC E7 (Merck) material was then injected to the empty cell inside a vacuum chamber. Under vacuum condition, the interstitial spaces of the TiO_2-IO films were easily infiltrated with the LCs due to the external pressure and capillary force.

2.6 Characterization

The morphology, size distribution and composition of as-prepared nanocrystals were investigated by the field emission scanning electron microscopy (FESEM, Merlin, Zeiss) with an energy-dispersive X-ray spectrometer (EDS). The compositions of films were characterized by X-ray diffraction (XRD) using a Bruker by X-ray diffraction (XRD) in a D8 advance X-ray diffractometer (Bruker, Switzerland) at a scanning rate of 0.2 °/min with a Cu Kα radiation (151.54056A °). Optical reflection spectra were measured with an unpolarized probe light beam using a UV-Vis-NIR microspectrophotometer (20/30 PV^{TM}, CRAIC). The broadband light beam was focused to have a probing area of 10 × 10 μm^2 using a 10 × objective lens combined with a variable aperture.

3. Results and discussion

Figure 2 shows FESEM images of the PS colloidal crystal fabricated by using a vertical self-assembly method [36]. A well-ordered 3D structure was clearly revealed from FESEM images with PS opals self-assembled with both 200 and 250 nm PS microspheres in diameter [Figs. 2(a) and 2(b)]. Figures 2(c) and 2(d) shows the resultant TiO_2-IOs after calcination with the estimated sizes in diameter of the spheroidal voids being ~180 nm and ~207 nm, respectively. Comparing to the corresponding PS spheres used in our experiments, there was a substantial decrease in diameter for the size of the spheroidal voids due to the shrinkage

Optics EXPRESS

during the calcination of PS spheres. It should be noted the shrinkage ratio varies a little for these two different sizes of PS spheres.

Figure 3(a) shows the XRD spectra of TiO_2-IOs sample and typical characteristic peaks from anatase TiO_2 nanocrystals can be observed. The strong diffraction peaks located at 2θ values of 25.3°, 37.8°, 48.1°, 53.9°, and 55.1°, which can be assigned to (101), (004), (200), (105), and (211) reflections of anatase TiO_2 nanocrystals, respectively [14]. Figure 3(b) shows the EDS spectra of the TiO_2-IOs sample, which confirms that Ti and O are the major elements. In addition, there exist signals for elemental Si, Ca, Na, and Pt in the EDS spectra, which come mainly from the FTO glass substrate, and the thin conducting layer (i.e., Pt) with the purpose for SEM observation.

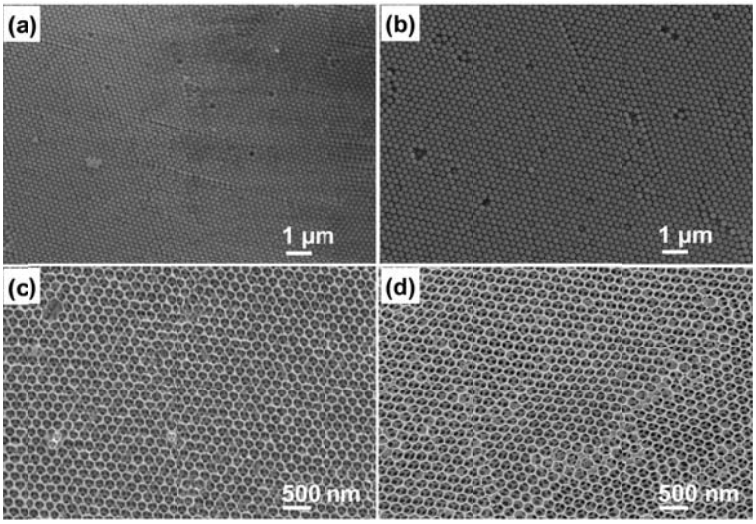

Fig. 2. FESEM images of PS colloidal crystal templates fabricated with the sphere size of 200 (a) and 250 nm (b) in diameter, and their corresponding TiO_2-IO films with the spheroidal void size of ~180 nm (c) and ~207 nm (d) replicated from PS opals.

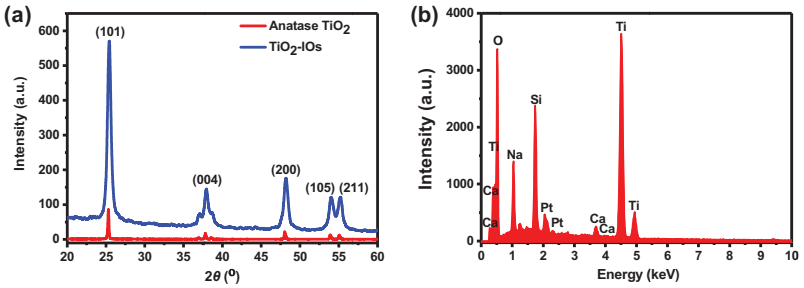

Fig. 3. The XRD pattern (a) and the EDS spectra (b) of TiO_2-IOs.

Optics EXPRESS

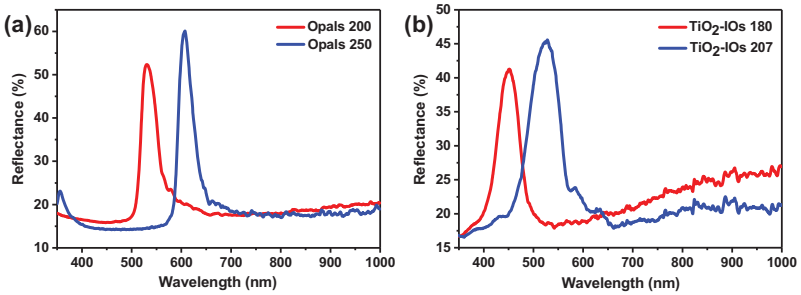

Fig. 4. Reflection spectra of PS templates (a) and TiO_2-IOs (b).

In our experiments, we prepared the PS opal templates and their corresponding TiO_2-IO samples using the PS spheres with two different sizes of 200 nm (PS opals-200) and 250 nm (PS opals-250) in diameter. Figure 4 shows the measured reflection spectra of PS opals and TiO_2-IO films, respectively. Distinct Bragg reflection peaks of PS opals-200 and PS opals-250 appear at 531 nm and 607 nm on the reflection spectra, respectively [Fig. 4(a)], indicating a well-ordered structure of the PS opals. Figure 4(b) shows the reflection spectra of the TiO_2-IO films. The Bragg reflection peaks of TiO_2-IOs from the 200-nm and 250-nm PS opal templates appear at 452 nm and 528 nm, respectively, showing a significant blue-shift. The blue-shift is caused by the decreased effective refractive index and reduced pore sizes.

As previously discussed, the fabricated TiO_2-IOs are closely packed face-centered cubic (FCC) PhCs. Under normally incident probe light, the Bragg reflectance results from the first order diffraction from the (111) planes of the IO structures. The reflectance peak for the (111) plane of a FCC lattice can be analytically determined by Bragg's law, as follows [33]:

$$\lambda_{\max} = \left(8/3\right)^{1/2} D\left(n_{\text{eff}}^2 - \sin^2\theta\right)^{1/2}, \tag{1}$$

where λ_{max} is the wavelength of stop band maximum, D is the diameter of the sphere/nanovoid, n_{eff} is the effective refractive index, and θ is the angle between the incident and the reflective surface.

By using the Bragg diffraction equation, we calculated the stop bands of both PS opals and TiO_2-IOs. For PS opals, according to the FCC crystal lattice, we assume that the volume fraction of PS is 74% while the volume fraction of air is 26%. The λ_{max} of PS opals-200 and PS opals-250 is calculated to be 475 nm and 594 nm, respectively [here it was assumed that the refractive index of PS is 1.59 and the refractive index of air is 1, thus $n_{eff} = (1.59^2 \times 0.74 + 1^2 \times 0.26)^{1/2} = 1.460$]. While for the corresponding TiO_2-IOs, λ_{max} is calculated to be 465 nm and 536 nm, respectively [here it was assumed that the refractive index of TiO_2 is 2.61 and the refractive index of air is 1, thus $n_{eff} = (1^2 \times 0.74 + 2.61^2 \times 0.26)^{1/2} = 1.585$]. We notice that the calculated stop band wavelengths for both PS opals and TiO_2-IOs do not match well with the measured ones, which could be mainly attributed to two major possible reasons: 1) the assumed volume ratio varies due to the shrinkage; and 2) the assumed refractive indices of PS and TiO_2 should be larger than the actual case.

Optics EXPRESS

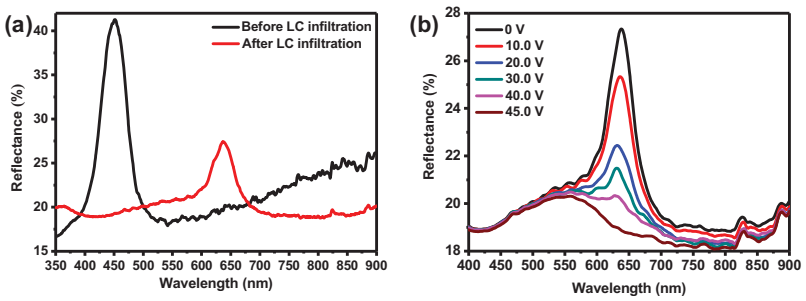

Fig. 5. (a) Reflection spectra of TiO_2-IOs before and after LC infiltration. (b) Reflection spectra measured at different voltage.

Compared to both opals structure and inverse opals structure, the structure provides a much less constricting volume for LC reorientation under applied fields, which should facilitate the largest possible optical tuning [37]. The sample was infiltrated with LC (E7) using an oven. Figure 5(a) shows the measured reflection spectra before and after LC infiltration for the TiO_2-IOs with a pore size of 180 nm. Before LC infiltration, the TiO_2-IOs showed a Bragg reflection peak at 452 nm and exhibited a full-width at half-maximum (FWHM) of 51 nm. Upon LC infiltration, the reflection peak red-shifted from 452 nm to 636 nm with a FWHM of 48 nm. The red-shift of the Bragg reflection peak can be attributed to the increase in the average refractive index of the film resulted from the replacement of air with LCs. Moreover, there is a significant decrease in reflectance due to the decreased refractive index contrast for the LC-infiltrated case, which is in good agreement with the expectation that the Bragg reflection peak collapses when the effective refractive indices between the spheroidal LC droplets and TiO_2 completely match each other. It is worth mentioning that there was no alignment layer in our experiments. We assumed that the LC molecules inside the voids were randomly aligned, hence demonstrating an averaged refractive index.

One distinctive feature for the LC-filtrated TiO_2-IOs is that the LC molecules can be realigned by an external electric field, making their optical properties switchable/tunable. Upon applying a voltage, the LC molecules inside the spheroidal voids can realign along the electric field direction, hence changing the effective refractive index of the LC. Once the applied voltage is removed, the LC molecules will return back to the original state. As a result, the refractive index contrast between the LCs and TiO_2 can be reversibly changed, hence leading to the change of the PBG properties. In our experiments, the reflectance spectra of one sample were measured as a function of applied AC voltage with the frequency of 25 kHz, as shown in Fig. 5(b). With the applied voltage, the Bragg peak continuously blue-shifts. With the increase voltages from 0 to 45 V, the Bragg peak demonstrates a slight blue-shift; more importantly, the reflection peak becomes much flat. We can see that the stop band could be completely switched at the voltage of 45 V, indicating a complete index match between LCs and TiO_2. At the driving voltage of 45 V, the measured rising and falling times were 5.5 and 3.0 ms, respectively. This complete switching behavior is different from the previous report [38], making it potentially useful for filtering application. It is worth noting that after switching off the Bragg peak, there still exists a broad peak with the center wavelength locating at ~550 nm. This broad peak may come from multilayer interference in the LC-filtrated TiO_2-IOs.

4. Conclusion

In conclusion, we have fabricated 3D macroporous anatase TiO_2-IOs from the PS opal templates through a sandwich vacuum backfilled method and followed by calcination. By infiltrating the TiO_2-IOs with a nematic LC, we have demonstrated electrically switchable

PhCs. The LC-infiltrated TiO_2-IOs possess a distinctive Bragg reflectance. Upon applying an external electric field, the Bragg reflectance peak can be switched due to the reorientation of the LC molecules inside the spherical voids. With advantageous features of low-cost fabrication, simple integration, and electric control, such LC-infiltrated TiO_2-IOs could play an important role in future development of active photonic devices, such as switches [39], filters [40,41], and structural colors [42,43].

Funding

Natural Science Foundation of Guangdong Province (Grant No. 2017A030313034 and 2018A030310224), Shenzhen Science and Technology Innovation Council (Grant No. JCYJ20170817111349280 and KQTD2016030111203005), National Natural Science Foundation of China (Grant No. 61805113), and Guangdong Innovative and Entrepreneurial Research Team Program (Grant No. 2017ZT07C071), and the joint French-Singaporean MERLION program (Grant No. R279000334133).

Acknowledgments

The authors thank the Key Laboratory of Municipal Solid Waste Recycling Technology and Management of Shenzhen City, Southern University of Science and Technology (SUSTech) for use of their facilities and equipment.

References

1. J. D. Joannopoulos, S. G. Johnson, J. N. Winn, and R. D. Meade, *Photonic Crystals: Molding the Flow of Light, 2nd Edition* (Princeton University Press, 2008).
2. Z. Cai, Z. Xiong, X. Lu, and J. Teng, "In situ gold-loaded titania photonic crystals with enhanced photocatalytic activity," J. Mater. Chem. A Mater. Energy Sustain. **2**(2), 545–553 (2014).
3. X.-Y. Yang, L.-H. Chen, Y. Li, J. C. Rooke, C. Sanchez, and B.-L. Su, "Hierarchically porous materials: synthesis strategies and structure design," Chem. Soc. Rev. **46**(2), 481–558 (2017).
4. K. Min, S. Kim, and S. Kim, "Deformable and conformal silk hydrogel inverse opal," Proc. Natl. Acad. Sci. U.S.A. **114**(24), 6185–6190 (2017).
5. R. A. Pala, J. White, E. Barnard, J. Liu, and M. L. Brongersma, "Design of plasmonic thin-film solar cells with broadband absorption enhancements," Adv. Mater. **21**(34), 3504–3509 (2009).
6. J. F. Galisteo-López, M. Ibisate, R. Sapienza, L. S. Froufe-Pérez, A. Blanco, and C. López, "Self-assembled photonic structures," Adv. Mater. **23**(1), 30–69 (2011).
7. S. D. Standridge, G. C. Schatz, and J. T. Hupp, "Toward plasmonic solar cells: protection of silver nanoparticles via atomic layer deposition of TiO_2," Langmuir **25**(5), 2596–2600 (2009).
8. X. Yang, Z. Peng, H. Zuo, T. Shi, and G. Liao, "Using hierarchy architecture of Morpho butterfly scales for chemical sensing: Experiment and modeling," Sens. Actuators A Phys. **167**(2), 367–373 (2011).
9. Z. Cai, D. H. Kwak, D. Punihaole, Z. Hong, S. S. Velankar, X. Liu, and S. A. Asher, "A photonic crystal protein hydrogel sensor for candida albicans," Angew. Chem. Int. Ed. Engl. **54**(44), 13036–13040 (2015).
10. Z. Cai, A. Sasmal, X. Liu, and S. A. Asher, "Responsive photonic crystal carbohydrate hydrogel sensor materials for selective and sensitive lectin protein detection," ACS Sens. **2**(10), 1474–1481 (2017).
11. H. Zhang and C. Cheng, "Three-dimensional FTO/TiO_2/$BiVO_4$ composite inverse opals photoanode with excellent photoelectrochemical performance," ACS Energy Lett. **2**(4), 813–821 (2017).
12. X. An, H. Lan, R. Liu, H. Liu, and J. Qu, "Light absorption modulation of novel Fe_2TiO_5 inverse opals for photoelectrochemical water splitting," New J. Chem. **41**(16), 7966–7971 (2017).
13. S. S. Mathew, S. Ma, and I. Kretzschmar, "Three-dimensionally ordered macroporous TiO_2 electrodes: Fabrication of inverse TiO_2 opals for pore-size-dependent characterization," J. Mater. Res. **28**(3), 369–377 (2013).
14. M. Zhou, C. Hou, J. Chen, J. Jin, L. Ju, S. Xu, C. Yao, and Z. Li, "Controlling the size of connecting windows in three-dimensionally ordered macroporous TiO_2 for enhanced photocatalytic activity," J. Mater. Sci. Mater. Electron. **29**(14), 11972–11981 (2018).
15. D. P. Gaillot, E. Graugnard, J. S. King, and C. J. Summers, Tunable electro-optic photonic crystals fabricated through template directed multilayer atomic layer deposition, SPIE Proc. **6182**, 61820Y (2006).
16. J. Liu, H. Zhao, M. Wu, B. Van der Schueren, Y. Li, O. Deparis, J. Ye, G. A. Ozin, T. Hasan, and B.-L. Su, "Slow photons for photocatalysis and photovoltaics," Adv. Mater. **29**(17), 1605349 (2017).
17. G. I. N. Waterhouse and M. R. Waterland, "Opal and inverse opal photonic crystals: Fabrication and characterization," Polyhedron **26**(2), 356–368 (2007).
18. M. Zalfani, B. van der Schueren, M. Mahdouani, R. Bourguiga, W.-B. Yu, M. Wu, O. Deparis, Y. Li, and B.-L. Su, "ZnO quantum dots decorated 3DOM TiO_2 nanocomposites: Symbiose of quantum size effects and photonic

Optics EXPRESS

structure for highly enhanced photocatalytic degradation of organic pollutants," Appl. Catal. B **199**, 187–198 (2016).
19. M. Zalfani, B. van der Schueren, Z.-Y. Hu, J. C. Rooke, R. Bourguiga, M. Wu, Y. Li, G. van Tendeloo, and B.-L. Su, "Novel 3DOM $BiVO_4/TiO_2$ nanocomposites for highly enhanced photocatalytic activity," J. Mater. Chem. A Mater. Energy Sustain. **3**(42), 21244–21256 (2015).
20. H. Zhang, G. Chen, and D. W. Bahnemann, "Photoelectrocatalytic materials for environmental applications," J. Mater. Chem. **19**(29), 5089–5121 (2009).
21. O. Bunsho, "Preparing articles on photocatalysis—Beyond the illusions, misconceptions, and speculation," Chem. Lett. **37**(3), 216–229 (2008).
22. A. Fujishima, X. Zhang, and D. A. Tryk, "TiO_2 photocatalysis and related surface phenomena," Surf. Sci. Rep. **63**(12), 515–582 (2008).
23. K. Lee and S. A. Asher, "Photonic crystal chemical sensors: pH and ionic strength," J. Am. Chem. Soc. **122**(39), 9534–9537 (2000).
24. J. H. Holtz and S. A. Asher, "Polymerized colloidal crystal hydrogel films as intelligent chemical sensing materials," Nature **389**(6653), 829–832 (1997).
25. Y. J. Liu and X. W. Sun, "Electrically tunable two-dimensional holographic photonic crystal fabricated by a single diffractive element," Appl. Phys. Lett. **89**(17), 171101 (2006).
26. Y. J. Liu and X. W. Sun, "Electrically tunable three-dimensional holographic photonic crystals made of polymer-dispersed liquid crystal," Jpn. J. Appl. Phys. **46**, 6634–6638 (2007).
27. Y. J. Liu, H. T. Dai, E. S. P. Leong, J. H. Teng, and X. W. Sun, "Electrically switchable two-dimensional photonic crystals made of polymer-dispersed liquid crystals based on the Talbot self-imaging effect," Appl. Phys. B **104**(3), 659–663 (2011).
28. S. Kubo, Z.-Z. Gu, K. Takahashi, Y. Ohko, O. Sato, and A. Fujishima, "Control of the optical band structure of liquid crystal infiltrated inverse opal by a photoinduced nematic-isotropic phase transition," J. Am. Chem. Soc. **124**(37), 10950–10951 (2002).
29. S. Kubo, Z.-Z. Gu, K. Takahashi, A. Fujishima, H. Segawa, and O. Sato, "Tunable photonic band gap crystals based on a liquid crystal-infiltrated inverse opal structure," J. Am. Chem. Soc. **126**(26), 8314–8319 (2004).
30. Y. J. Liu, Y. B. Zheng, J. Shi, H. Huang, T. R. Walker, and T. J. Huang, "Optically switchable gratings based on azo-dye-doped, polymer-dispersed liquid crystals," Opt. Lett. **34**(15), 2351–2353 (2009).
31. Y. J. Liu, H. T. Dai, E. S. P. Leong, J. H. Teng, and X. W. Sun, "Azo-dye-doped absorbing photonic crystals with purely imaginary refractive index contrast and all-optically switchable diffraction properties," Opt. Mater. Express **2**(1), 55–61 (2012).
32. Y. J. Liu, Z. Cai, E. S. P. Leong, X. S. Zhao, and J. H. Teng, "Optically switchable photonic crystals based on inverse opals partially infiltrated by photoresponsive liquid crystals," J. Mater. Chem. **22**(15), 7609–7613 (2012).
33. Z. Cai, J. Teng, Z. Xiong, Y. Li, Q. Li, X. Lu, and X. S. Zhao, "Fabrication of TiO_2 binary inverse opals without overlayers via the sandwich-vacuum infiltration of precursor," Langmuir **27**(8), 5157–5164 (2011).
34. S. E. Shim, Y. J. Cha, J. M. Byun, and S. Choe, "Size control of polystyrene beads by multistage seeded emulsion polymerization," J. Appl. Polym. Sci. **71**(13), 2259–2269 (1999).
35. E. Eftekhari, P. Broisson, N. Aravindakshan, Z. Wu, I. S. Cole, X. Li, D. Zhao, and Q. Li, "Sandwich-structured TiO_2 inverse opal circulates slow photons for tremendous improvement in solar energy conversion efficiency," J. Mater. Chem. A Mater. Energy Sustain. **5**(25), 12803–12810 (2017).
36. P. Jiang, J. F. Bertone, K. S. Hwang, and V. L. Colvin, "Single-crystal colloidal multilayers of controlled thickness," Chem. Mater. **11**(8), 2132–2140 (1999).
37. I. C. Khoo, Y. Williams, A. Diaz, K. Chen, J. A. Bossard, L. Li, D. H. Werner, E. Graugnard, J. S. King, S. Jain, and C. J. Summers, "Liquid-crystals for tunable photonic crystals, frequency selective surfaces and negative index material development," Mol. Cryst. Liq. Cryst. (Phila. Pa.) **453**(1), 309–319 (2006).
38. E. Graugnard, S. N. Dunham, J. S. King, D. Lorang, S. Jain, and C. J. Summers, "Enhanced tunable Bragg diffraction in large-pore inverse opals using dual-frequency liquid crystal," Appl. Phys. Lett. **91**(11), 111101 (2007).
39. Y. J. Liu, X. W. Sun, J. H. Liu, H. T. Dai, and K. S. Xu, "A polarization insensitive 2×2 optical switch fabricated by liquid crystal-polymer composites," Appl. Phys. Lett. **86**(4), 041115 (2005).
40. Y. J. Liu, G. Y. Si, E. S. P. Leong, N. Xiang, A. J. Danner, and J. H. Teng, "Light-driven plasmonic color filters by overlaying photoresponsive liquid crystals on gold annular aperture arrays," Adv. Mater. **24**(23), OP131–OP135 (2012).
41. S. T. Yin, Y. J. Liu, D. Xiao, H. L. He, D. Luo, S. Z. Jiang, H. T. Dai, W. Ji, and X. W. Sun, "Liquid-crystal-based tunable plasmonic waveguide filters," J. Phys. D Appl. Phys. **51**(23), 235101 (2018).
42. S. Kim, A. N. Mitropoulos, J. D. Spitzberg, H. Tao, D. L. Kaplan, and F. G. Omenetto, "Silk inverse opals," Nat. Photonics **6**(12), 818–823 (2012).
43. S. Y. Lee, S.-H. Kim, H. Hwang, J. Y. Sim, and S.-M. Yang, "Controlled pixelation of inverse opaline structures towards reflection-mode displays," Adv. Mater. **26**(15), 2391–2397 (2014).